Structures and Phases in (Nano-)Systems in Confined Geometry

M. Beck, A. Haller, D. Kawetzki, M. Matt, M. Pütz, M. Ring, R. Schmid, K. Scholz, U. Siems, P. Nielaba

published in

NIC Symposium 2016
K. Binder, M. Müller, M. Kremer, A. Schnurpfeil (Editors)

Forschungszentrum Jülich GmbH,
John von Neumann Institute for Computing (NIC),
Schriften des Forschungszentrums Jülich, NIC Series, Vol. 48,
ISBN 978-3-95806-109-5, pp. 229.
http://hdl.handle.net/2128/9842

Structures and Phases in (Nano-)Systems in Confined Geometry

Marcus Beck, Andreas Haller, Daniel Kawetzki, Manuel Matt, Martin Pütz, Markus Ring, Ralf Schmid, Kristian Scholz, Ullrich Siems, and Peter Nielaba

Department of Physics, University of Konstanz, 78457 Konstanz, Germany
E-mail: {marcus.beck, andreas.haller, daniel.kawetzki, manuel.matt, martin.puetz, markus.ring, ralf.schmid, kristian.scholz, ullrich.siems, peter.nielaba}@uni-konstanz.de

Computer simulations by members of the NIC-project HMZ07 are reviewed. Structural and transport properties have been investigated in atomic wires by Molecular Dynamics and electronic transport methods and in model colloids by Brownian Dynamics. Nano-alloys and nano-resonators have been analysed by Molecular Dynamics and path integral Monte Carlo. Spinodal decomposition and domain growth of liquid-vapour systems and galaxy magnetism have been studied by hydrodynamics simulations, and nucleation phenomena in lattice systems by rare event methods.

1 Introduction

Nanostructures and colloidal systems in reduced geometry and external fields have become an interesting research domain in the last years, and in this field, computer simulation studies have contributed many important results. Here we review results obtained in our NIC project HMZ07 and present recent results.

In Sec. 2, we report on the computations of electronic and structural properties of atomic wires. In Sec. 3, the effects of external periodic light fields and driving forces on the structural and dynamical properties of two dimensional colloidal systems, confined in a channel geometry, are analysed by Brownian Dynamics simulations as well as the effect of counterflow on segregation phenomena and the ordering on non-spherical particles in channel geometry. In Sec. 4, the properties of nano-alloys and of nano-resonators in the beam geometry are discussed. Effects of the system size and stretching on the resonator frequencies and damping constants have been computed by Molecular Dynamics, and quantum effects at low temperatures by path integral Monte Carlo. In Sec. 5, hydrodynamics simulations for spinodal decomposition phenomena and galaxy magnetism are presented, and in Sec. 6, results for nucleation phenomena in lattice systems, obtained by rare event methods.

2 Control of Properties of Atomic-Sized Contacts

The potential to construct electronic devices with functional building blocks of atomic size is a major driving force of nanotechnology. When wires are stretched to structures, where only few atoms connect the two ends of the wire, interesting current quantisation phenomena occur. In collaborative work, involving J. C. Cuevas, F. Pauly, E. Scheer, and others, in recent studies[1–4] we investigated the structural and electronic properties of atomic wires. For the Molecular Dynamics (MD) simulations we used the open source program package

LAMMPS[5]. Within LAMMPS, we employed the Embedded Atom Method (EAM) with the semi-empirical potentials from Sheng *et al.*[6] to model the interactions between the atoms. To calculate the transport properties of the geometries obtained from the MD simulations, the Landauer-Büttiker formalism was used. We expressed it in terms of Green's function techniques, as explained in Refs. 7, 4. According to the Landauer formula, the

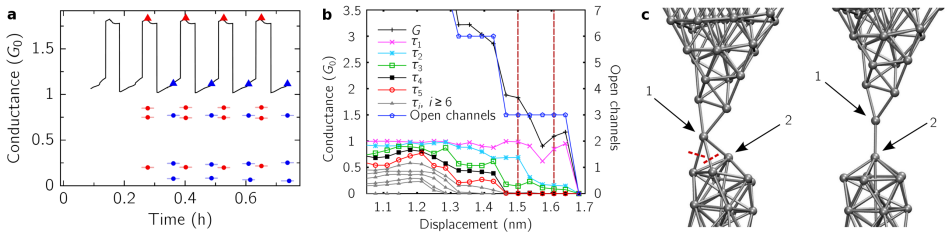

Figure 1. (a) Experimental results from a switching process. (b) A conductance trace G with its channel contributions τ_i as function of the displacement of the two leads from its ideal structure. (c) Connected structures which would explain the experimental findings[3].

transmission eigenchannels τ_i are related to the conductance via $G = G_0 \sum_i \tau_i$, where $G_0 = 2e^2/h$ is the quantum of conductance. Conductance histograms for aluminium wires have been compared with experimental data[3]. Further on we used the information of the channels of the individual traces to connect the experimental results with information about atomic configurations. An example is given in Fig. 1, where in (a) one can find the experimental results from the switching process, in (b) a conductance trace with its channel contributions as function of the displacement of the two leads, and in (c) the connected structures which would explain the experimental findings, are shown. With this formalism we have also access to other properties like shot noise, Fano factor[2] and thermopower[1]. With statistics of 100 curves each we compared conductance histograms, Fano factor, shot noise and thermopower data with experimental results and supported them further with channel distribution data and atomic configurations. With this, we were able to explain[2] a peak in the variance of the shot noise experiments of Au at about $0.5G_0$. This peak indicates the contribution of more than one channel. Our studies showed low probability appearances of more than one wire in parallel contributing with one channel less than one G_0. In Ref. 1 we showed, in agreement with experiments, that both Au and Pt statistically have a non vanishing thermopower while going from big contacts to single atom contacts, but with different sign. We could explain the different sign with the help of energy dependent transmission calculations $\tau(E)$ and the calculation of the local density of states (DOS) in the central region of the contacts.

3 Colloidal Systems

Colloidal particles in two- and three-dimensional micro-channels have been studied by Brownian Dynamics (BD) simulations[8–12], where the particle interactions were modelled by dipolar or Yukawa interactions and hard or soft core potentials with particle diameter σ

for the treatment of the particles excluded volume, and the particle-wall interactions by several methods[13,14]. Interesting layering phenomena as function of the channel width were detected in two dimensional systems[8], in good agreement with experimental studies[8], and are predicted for three dimensional systems[9]. An analysis of the particles diffusion properties in channel direction revealed a non-monotonic crossover from single-file to regular diffusion[10], in close agreement with experimental results[10].

In a recent study[11] we examined the effect of a sinusoidal washboard potential on the structure and transport properties of a colloidal system in channel geometry, in order to contribute to the analysis of recent related experimental studies[15]. In addition to the driving force F, an external force, periodic in x direction, was applied: $F_x = F + F_p \sin\left(\frac{2\pi}{\lambda}x\right)$. Here, F_p is the amplitude of the periodic force and λ the period length in x-direction.

Without a substrate potential, the particle velocity would equal the applied force. With a substrate potential, the mean velocity is clearly reduced compared to the case of a free moving particle. For small forces the motion of the particles is similar to that in a pinned case. At a certain threshold force the particles start to move, and for high forces the velocity slowly merges into the free velocity. For small period lengths, the particles order more in a triangular structure and for large periods $\lambda > 1.5$, a rectangular order can be identified, see Fig. 2. The layering is only suppressed around $\lambda = 1.5$. For small as well as for large period lengths, four layers are well pronounced, for $\lambda = 0.9$, each second minimum at the boundary is occupied by a particle. For $\lambda = 2.1$, a very strong increase in the mobility at low forces occurs. This is due to very mobile boundary particles that are located between two minima. These topological defects are localised on a few particles around the extra particle and are the so-called "kink" solitons, as known from the Frenkel-Kontorova model.

The effect of counterflow in model colloids has been investigated as well by BD methods: (a) In a recent study[12], segregation phenomena of particles driven in opposite directions have been studied. The particles interacted via a repulsive potential and were confined in three-dimensional hard-walled pipes with quadratic cross sections. In a systematic finite-size study, the pipe length was varied. Ordering on finite length scales was found, but global segregation seems to vanish for infinite channel length, as it was recently found for lane formation in two dimensions. As an additional effect of the finite hard-walled boundary conditions, interface vibrations and longitudinal demixing were found. (b) In another study[16], we considered channels with radial symmetry. The particles were confined in a hollow cylinder with inner radius R_{min}, outer radius R_{max} and height H with quadratic cross section (Fig. 2(b) $R_{max} - R_{min} = H = 9.5$). The two particles types were driven against each other by a radial force $F = F_{max}(R/R_{max})$, acting on each particle in such a way, that the particles moved with a constant angular velocity. At a force of about $F_{max} = 60$ the particles segregated into an inner ring and an outer ring of one particle type, moving in opposite directions (see Fig. 2(b)).

In a recent study, we investigated the layering behaviour of hard spherocylinders in channel geometry[17]. The spherocylinders interacted by the Kihara potential[18] and were confined by soft walls. A strong effect of the channel width on the particles ordering (see Fig. 2(c)) and their dynamics was found, similar to previous findings for spherical particles. Detailed further investigations of structural and dynamical properties of mixtures with spherical particles and of finite site effects are planned by a variation of aspect ratios and channel widths, in order to achieve a better understanding of the ordering effect of the confinement on structural and dynamical properties of such systems.

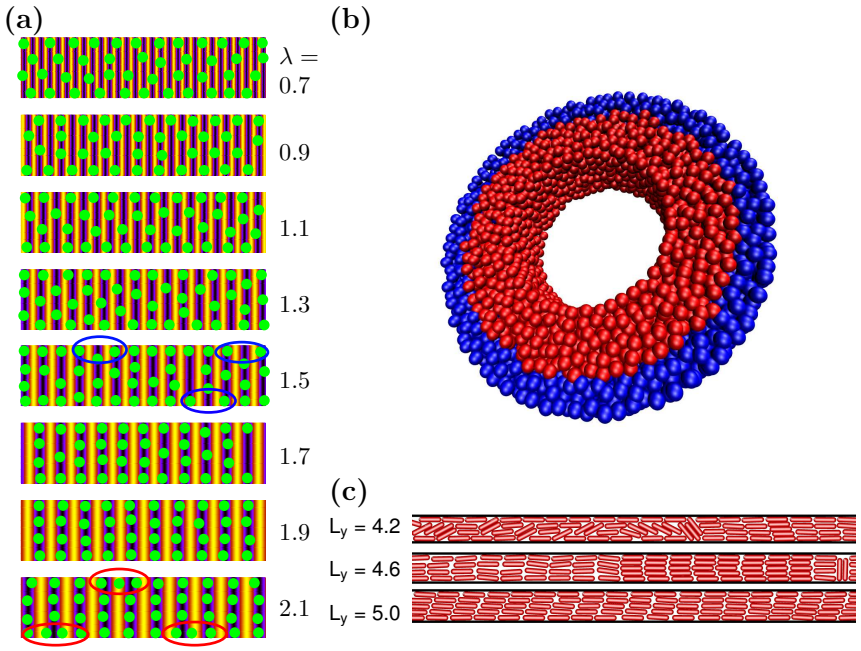

Figure 2. (a) Snapshots of the equilibrium positions for different period lengths (λ=0.7, 0.9, 1.1, 1.3, 1.5, 1.7, 1.9, 2.1 from top to bottom) on the colour-coded substrate potential (bright, maximum; dark, minimum). Red ellipses, kinks; blue ellipses, antikinks. (b) Snapshot of ordered oppositely driven particle on a ring geometry. (c) Typical configurations for spherocylinders with aspect ratio 5 for various channel wall distances L_y.

4 Nano-Alloys and Nano-Resonators

Due to their remarkable mechanical properties upon loading followed by heating ["shape memory effect" (SME)] and vice versa ["superelasticity" (SE)], shape memory alloys (SMAs) are widely applied these days in diverse macroscopic engineering devices[19]. Microscopically, these effects result from the martensitic phase transformation between crystal structures of different symmetries, and from the formation of differently oriented variants of the low-temperature ground state phase ("martensite").

In our project, atomistic simulation methods (Molecular Dynamics) have been developed and utilised to compute the phase diagram of NiTi[20] and FeNi alloys, the effect of the system size on the transition temperature in nano-scale systems[21], and a full thermodynamic cycle of a temperature driven nano-motor[22]. The phase transition temperatures for $Ni_{50}Ti_{50}$ obtained in our studies were in excellent agreement with the experimental data.

The properties of nano-beam resonators have attained much attention recently[23], due to their experimental realisation and the investigation of their properties at sub micro-metre length scales[24] accompanied by analytical approximations and computer simulations[25,26].

The experimentally studied systems typically show a temporal decay of the oscillation amplitude. Here we report on results of systematic atomistic MD simulations of the dynamical properties of oscillating resonators of various geometries at the nanometre length scale

for various temperatures, under the influence of external stresses, and with local vacancies, using the program SEEVN, developed in our project[27], or by the package LAMMPS[5]. Since we are interested in general properties of beam resonator systems, we studied and compared the properties of three systems: Si, SiN, and NiTi, accompanied by studies of systems with simple Lennard-Jones interactions. Our systems are modelled by well tested interaction potentials[28,29,25].

In our studies[27], we have found interesting structural properties, like a 2x1 dimer surface- and an edge-reconstruction in Si nano-beams, as well as interesting dynamical properties, which are qualitatively similar in all systems studied, but may vary in magnitude due to the different particle interactions. Typical beam sizes were 10-30 nm in length and 2-4 nm in width corresponding to a few thousand up to several ten thousand atoms. After the initial preparation of the structures, the beams were deflected by applying a force until the maximum deflection was obtained, followed by a free oscillation of the beams[27]. Whenever thermalisation was required in order to heat the beams to a specific temperature, either an Andersen or a Langevin thermostat was used. The end points of the beam were kept fixed. From the time evolution of the centre of mass coordinates we obtained the oscillation frequency f and damping coefficient γ either by Fourier transformation or by directly fitting the resulting curve to an exponentially damped oscillation according to $A\exp(-\gamma t)\sin(2\pi ft-\varphi)+c$.

Fig. 3 shows the high and low frequency parts of the kinetic energy for a NiTi beam for its first and 150th period of oscillation. The energy of the collective motion decreases significantly and dissipates into the fluctuations of the individual atoms around their local lattice positions of the constituting atoms. Fig. 3 (c) shows histograms of the high frequency part of the x coordinate of an atom in the centre of a NiTi beam for the same two periods of oscillation. At the start of the oscillation, the distribution is sharp due to the collective motion. During the oscillations, the distribution broadens, see Fig. 3(c), due to the local energy flow from the collective mode into the fluctuations of the individual atoms around their local lattice positions, which results in an increase of occupied phase space Γ of the single atoms, and therefore an increase in entropy according to $S \propto \ln\Gamma$. For the collective mode this mechanism results in a damping.

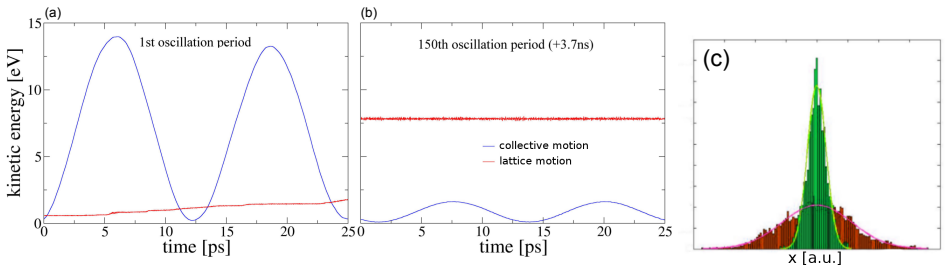

Figure 3. (a) and (b) High (red) and low (blue) frequency parts of the kinetic energy of a NiTi beam summed over all atoms. (a) first oscillation period. (b) 150th oscillation period (after 3.7 ns of oscillation). (c) Normalised histograms of the high frequency part of the x coordinate of an atom in the centre of a NiTi beam for the first (green) and 150th (orange) period of oscillation.

A systematic variation of the system sizes, temperatures and external stresses revealed a strong frequency increase by external stress, e.g. an increase from about 45 GHz to about 62 GHz in Si-beams (with 4x4x60 unit cells) by a 12 % stretching of the wire, a decrease of f with increasing temperature, an increase of the damping coefficient with the temperature and a decrease of the damping with increasing stress. The frequency depends on the beam length L nearly as $1/L^2$, in agreement with the Euler-Bernoulli beam theory.

Quantum effects

A method for the computation of low temperature materials properties is the path integral

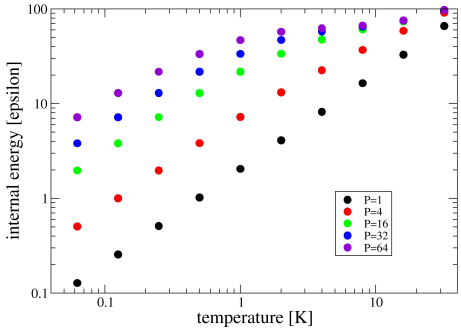

Figure 4. Internal energy of a 100 atom chain with fixed end points for different Trotter numbers P. With increasing Trotter number, the data scale to the quantum limit, resulting in proper low temperature data[27].

Monte Carlo method, which has been successfully applied to study the low temperature properties of silicates, the effect of external light fields on the phase diagram of quantum disks, and related systems[31–34]. This method permits a systematic approach to the quantum limit, and thus - by comparison with purely classical simulations - the determination of the Debye temperature in nano-beams and -membranes, which is a goal of our project. Fig. 4 shows the internal energy of a 100 atom long Lennard-Jones chain with fixed end points. At low temperature, the classical linear temperature dependence (for Trotter number P=1) results in a wrong low temperature heat capacity, contradicting the third law of thermodynamics. With increasing Trotter number P, the results approach the correct low temperature quantum limit, which can be obtained by extrapolation for large P. By this method, such qualitative defects of classical computations can be cured. Our results also indicate that the average width of the chain shows characteristic differences.

5 Hydrodynamics Simulations

One goal of our NIC project is to develop a new method for hydrodynamics computations in soft matter systems using a smoothed particle approach as implemented in astrophysical codes (GADGET[35]). In colloidal dispersions, the solvent often is charged, resulting in

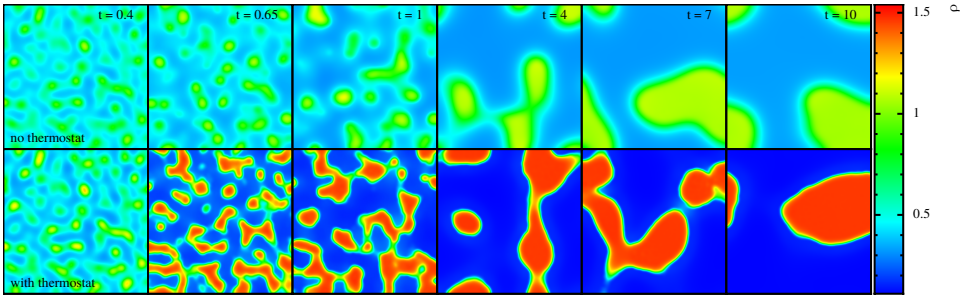

Figure 5. Comparison of density rendered cross section slices from simulation snapshots at the times $t = 0.4$, 0.65, 1.00, 4.00, 7.00, 10.00. The pure thermal simulations with no thermostat (top row) and with thermostat (bottom row), with a side length of the box size $L = 1$. Note that the actual shapes of the three dimensional structures can not be determined in the two dimensional representation.

long range forces. In addition, colloidal particles often are (para-) magnetic systems. The treatment of long range forces in continuum simulations has been optimised in codes like GADGET, and we plan to develop these methods further for systems with long range interactions (magnetic fields in galaxies) and to transfer these methods to condensed matter phenomena in systems with long range interactions at a later stage.

Spinodal decomposition with hydrodynamics

We successfully applied a modification of the massively parallelised astrophysical Smoothed Particle Hydrodynamics (SPH) code GADGET2 to simulations of spinodal decomposition of liquid-vapour systems[36]. The results are in excellent agreement with theoretical predictions for all expected time regimes from the initial growth of "homophase fluctuations" up to the inertial hydrodynamics regime. The numerical approach follows a modern formulation of the SPH method[37,38] with a van der Waals equation of state[39] and thermal conduction[40]. The dynamics and thermal evolution of instantaneously temperature-quenched systems are investigated. Therefore, we used a simple scaling thermostat that allows thermal fluctuations at a constant predicted mean temperature. Therefore the scaling approach is implemented in the way, that the new particle temperatures $\tilde{T}_i$ are given by $\tilde{T}_i = T_i \cdot (T_0/\overline{T})$, where $\overline{T}$ and T_0 are the mean and initial temperature, respectively.

We found that the initial stage spinodal decomposition is strongly affected by the temperature field. The separated phases react on density changes with a change in temperature. Although, the thermal conduction acts very slowly, thermal deviations are eventually compensated. The domain growth in the late stage of demixing is found to be rather unaffected by thermal fluctuations. We observe a transition from the Lifshitz-Slyozov growth rate with $1/3$ exponent to the inertial hydrodynamics regime with a rate of $2/3$, only excepted from simulations near the critical point where the liquid droplets are observed to nucleate directly in a spherical shape. A comparison of cross section slices of simulations with and without thermostat is shown in Fig. 5. The transition between the growth regimes when the thermostat is applied has been studied by simulations with several initial temperatures and is found to occur earlier for higher initial temperatures. We explain this time dependency with the phase interfaces that become more diffuse and

overlap with approaching the critical point. A prolonging behaviour of the demixing process is observed and also expected to depend on temperature. It is further found that the observations can excellently explain the growth behaviour for pure nonisothermal simulations that are performed without thermostat.

Magnetohydrodynamics simulations
Magnetic fields are an important property of virtually every astrophysical system. Thereby cooperative work between radio observations and theoretical work based on computer simulation plays an important role and is needed to constrain e.g. galactic magnetic fields and the physical processes responsible for its creation. We successfully applied the simulation code GADGET on a variety of astrophysical scenarios (e.g. star formation[41], protostellar outflow[41] and galaxy dynamics and interaction[42–44]). Many details concerning the influence of magnetic fields are still left to be explored due to the intrinsic complexity associated with the treatment of magnetohydrodynamics in numerical simulations. Detailed knowledge of the structure of our Galaxy from modelling and simulation is crucial for a variety of astrophysical questions, e.g. Ref. 45. For our simulations of the (gas) dynamics and their interplay with magnetic fields in galaxies we use the development version of GADGET[35], GADGET-3. Thereby, a state-of-the-art SPH formulation with improved accuracy for simulations of galaxies and the large-scale structure is used[46]. In order to investigate magnetic fields the smoothed particle magnetohydrodynamics implementation of Ref. 47 is used, and in a recent study[48] we investigated the small scale magnetic field of our own Galaxy, the Milky Way.

6 Nucleation Studies

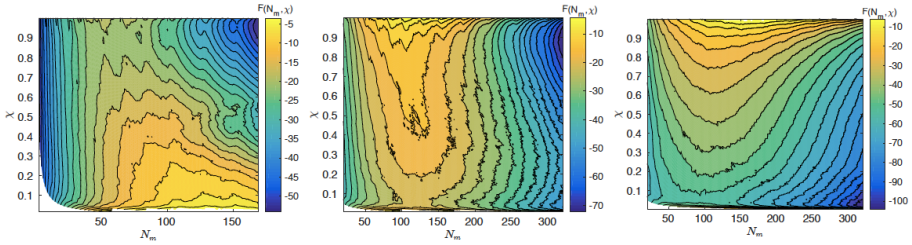

Figure 6. Free energy as function of the two component Potts model with cluster size N_m and crystallinity ratio χ for three temperatures: $k_BT = 0.6$ (left), $k_BT = 0.7$ (middle), $k_BT = 0.8$ (right)[55].

Based on Refs. 49, 51, 52, metadynamics[53], transition path sampling[50] and transition interface sampling[54] techniques have been used in a recent study[55], to compute structures of critical nuclei and nucleation rates in Ising and Potts models. As described in Ref. 49, at a temperature below the roughening transition, the critical nuclei in the Ising system have a rough and non-spherical structure. The novel application of metadynamics to the nucleation scenario in the Ising model[55] gave easy access to the free energy. Further application of the transition path ensemble[50] and transition interface sampling[54] methods were used to

compute nucleation rates[55]. The methods developed for the nucleation studies in the Ising model are transferred to the Potts model in our project. Nucleation phenomena based on a Potts model description have been studied in Refs. 51, 52. In a two component system with solvent and solute particles, lattice sites are occupied by one particle type with one of 24 possible orientations in a three dimensional cubic system. The Hamiltonian is given by Ref. 51: $H = -\sum_{k=1}^{2}\left[\sum_{\langle i,j\rangle}\left[\delta_{m(i),k}\delta_{m(j),k}\left(G_k + \delta_{s(i)s(j)}A_k\right)\right]\right]$. Here, $\langle i,j\rangle$ is the nearest neighbour summation convention, $m(i)$ is the particle type (1 or 2) and $s(i)$ the orientation of a particle at lattice site i, and A_k and G_k control the freezing points and solubilities of both components. In order to compare our results with Ref. 51, the values are chosen as $G_1 = G_2 = 1, A_1 = 1, A_2 = 0$. In a recent study[55], we could show that metadynamics can be easily applied to the nucleation scenario. The resulting free energy as a function of the particle number N_m of the largest cluster of the same component and of the number N_s of of particles with the same orientation s in this cluster, or the crystallinity ratio $\chi = N_s/N_m$, shows interesting features for different temperatures, see Fig. 6. For high temperatures, the nucleation can be described by an amorphous cluster growth (Fig. 6 (middle and right)), whereas at low temperature (Fig. 6(left)), first the cluster crystallises and then grows. These two different scenarios beautifully mirror the different experimentally observed nucleation and growth pathways, namely on the one hand via amorphous precursors versus on the other hand classical critical nuclei[56].

Acknowledgements

Discussions and collaborations are gratefully acknowledged to J. C. Cuevas, F. Pauly, E. Scheer, C. Schirm, N. Agraït, R. Chen, C. Evangeli, D. Natelson, L. Rincón-García, G. Rubio-Bollinger on the electronic transport studies, to B. Heinze, N. Schwierz, S. Sengupta, A. Erbe, P. Leiderer, C. Kreuter on the colloidal transport studies in channels, to D. Mutter on nano-alloys simulations, to A. Beck and K. Dolag on hydrodynamics simulations, and to C. Peter on nucleation studies. We thank the NIC for computer time on JUROPA / JURECA for the project HMZ07 and the SFBs 767, TR6 and 1214 for support.

References

1. C. Evangeli, M. Matt, L. Rincon-Garcia, F. Pauly, P. Nielaba, G. Rubio-Bollinger, J. C. Cuevas, N. Agrait, Nano Lett. **15**, 1006, 2015.
2. R. Chen, M. Matt, F. Pauly, P. Nielaba, J. C. Cuevas, D. Natelson, J. Phys. Cond. Mat. **26**, 474204, 2014.
3. C. Schirm, M. Matt, F. Pauly, J. C. Cuevas, P. Nielaba, E. Scheer, Nature Nanotech. **8**, 645, 2013.
4. F. Pauly, J. K. Viljas, M. Bürkle, M. Dreher, P. Nielaba, J. C. Cuevas, Phys. Rev. B **84**, 195420, 2011.
5. S. Plimpton, J. Comp. Phys. **117**, 1, 1995.
6. H. W. Sheng, M. J. Kramer, A. Cadien, T. Fujita, M. W. Chen, Phys. Rev. B **83**,134118, 2011.
7. M. Dreher, F. Pauly, J. Heurich, J. C. Cuevas, E. Scheer, P. Nielaba, Phys. Rev. B**72**, 075435, 2005.

8. M. Köppl, P. Henseler, A. Erbe, P. Nielaba, P. Leiderer, Phys. Rev. Lett. **97**, 208302, 2006.
9. N. Schwierz, P. Nielaba, Phys. Rev. E **82**, 031401, 2010.
10. U. Siems, C. Kreuter, A. Erbe, N. Schwierz, S. Sengupta, P. Leiderer, P. Nielaba, Sci. Rep. (Nature) **2** 1015, 2012.
11. U. Siems, P. Nielaba, Phys. Rev. E **91**, 022313, 2015.
12. B. Heinze, U. Siems, P. Nielaba, Phys. Rev. E **92**, 012323, 2015.
13. D. M. Heyes, J. R. Melrose, J. Non-Newtonian Fluid Mechanics **46**, 1, 1993.
14. H. Behringer, R. Eichhorn, Phys. Rev. E **83** 065701(R), 2011.
15. T. Bohlein, J. Mikhael, C. Bechinger, Nat. Mater. **11**, 126, 2011.
16. D. Kawetzki, Bachelor Thesis, University of Konstanz, 2014.
17. A. Haller, Bachelor Thesis, University of Konstanz, 2014.
18. T. Kihara, J. Phys. Soc. Japan **289**, 6, 1951.
19. D. C. Lagoudas(Ed.), *Shape Memory Alloys: Modeling and Engineering Applications*, Springer, 2010.
20. D. Mutter, P. Nielaba, Phys. Rev. B **82**, 224201, 2010.
21. D. Mutter, P. Nielaba, Eur. Phys. J. B **84**, 109, 2011.
22. D. Mutter, P. Nielaba, J. Alloys Compd. **577S**, S83, 2013.
23. A. N. Cleland, *Foundations of Nanomechanics*, Springer, 2002.
24. J. Rieger, A. Isacsson, M. J. Seitner, J. P. Kotthaus, E. M. Weig, Nature Comm. **5**,3345, 2014.
25. P. Vashishta, R. K. Kalia, A. Nakano, in *Handbook of Materials Modeling*, Springer, 2005.
26. M. Chu, R. E. Rudd, M. P. Blencowe, arXiv 0705:0015v1, 2007.
27. K. Scholz, Dissertation, University of Konstanz (in preparation).
28. F. H. Stillinger, T. A. Weber, Phys. Rev. B **31**, 5262, 1985.
29. J. Tersoff, Phys. Rev. B **37**, 6991, 1988.
30. M. Ring, Master Thesis, University of Konstanz, 2013.
31. M. H. Müser, P. Nielaba, K. Binder, Phys. Rev. B **51**, 2723, 1995.
32. C. Rickwardt, P. Nielaba, M. H. Müser, K. Binder, Phys. Rev B **63**, 045204, 2001.
33. J. Hoffmann, P. Nielaba, Phys. Rev. E **67**, 036115, 2003.
34. P. Nielaba, W. Strepp, in: *Path Integrals New Trends and Perspectives*, ed. by W. Janke and A. Prestel, World Scientific, Singapore, 321, 2008.
35. V. Springel, Mon. Not. R. Astron. Soc. **364**, 1105, 2005.
36. M. Pütz, P. Nielaba, Phys. Rev. E **91**, 032303, 2015.
37. V. Springel, Annu. Rev. Astron. Astrophys. **48**, 391, 2010.
38. D. J. Price, J. Comput. Phys. **231**, 759, 2012.
39. S. Nugent, and H. A. Posch, Phys. Rev. E **62**, 4968–4975, 2000.
40. M. Jubelgas, V. Springel, K. Dolag, Mon. Not. R. Astron. Soc. **351**, 423, 2004.
41. F. Bürzle, P. C. Clark, F. Stasyszyn, T. Greif, K. Dolag, R. S. Klessen, P. Nielaba, Mon. Not. R. Astron. Soc. **412**, 171, 2011.
42. A. Geng, H. Kotarba, F. Bürzle, K. Dolag, F. Stasyszyn, A. Beck, P. Nielaba, Mon. Not. R. Astron. Soc. **419**, 3571, 2012.
43. A. Geng, A. M. Beck, K. Dolag, F. Bürzle, M. C. Beck, H. Kotarba, P. Nielaba, Mon. Not. R. Astron. Soc. **426**, 3160, 2012.

44. A. Beck, H. Lesch, K. Dolag, H. Kotarba, A. Geng, F. Stasyszyn, Mon. Not. R. Astron. Soc. **422**, 2152, 2012.
45. K. Dolag, B. M. Gaensler, A. M. Beck, M. C. Beck, Mon. Not. R. Astron. Soc. **451**, 4277, 2015.
46. A. M. Beck, G. Murante, A. Arth, R.-S. Remus, A. F. Teklu, J. M. F. Donnert, S. Planelles, M. C. Beck, P. Förster, M. Imgrund, K. Dolag, S. Borgani, Mon. Not. R. Astron. Soc. **455**, 2110, 2016.
47. K. Dolag, F. Stasyszyn, Mon. Not. R. Astron. Soc. **398**, 1678, 2009.
48. M. C. Beck, A. M. Beck, R. Beck, K. Dolag, A. W. Strong, P. Nielaba, preprint (arXiv:1409.5120).
49. A. C. Pan, D. Chandler, J. Phys. Chem. B **108**, 19681, 2004.
50. P. G. Bolhuis, C. Dellago, D. Chandler, P. Geissler, Annu. Rev. Phys. Chem. **59**, 291, 2002.
51. N. Duff, B. Peters, J. Chem. Phys. **131**, 184101, 2009.
52. V. Agarwal, B. Peters, J. Chem. Phys. **140**, 084111, 2014.
53. A. Laio, M. Parrinello, Proc. Nat. Acad. Sci. U.S.A., **99**, 12562, 2002.
54. T. S. van Erp, D. Morioni, P. G. Bolhuis, J. Chem. Phys. **118**, 7762, 2003.
55. R. Schmid, Master Thesis, University of Konstanz, 2015.
56. D. Gebauer, H. Cölfen, Nano Today **6**, 564, 2011.